AGU PUBLICATIONS

JGR

Journal of Geophysical Research: Space Physics

BRIEF REPORT

10.1002/2013JA019557

Key Points:
- New emissions with line structures detected close to the ionospheric trough
- Most probably they are due to EMIC waves coming from the equatorial region
- They are common and observed during substorms

Correspondence to:
M. Parrot,
mparrot@cnrs-orleans.fr

Citation:
Parrot, M., F. Němec, and O. Santolík (2014), Analysis of fine ELF wave structures observed poleward from the ionospheric trough by the low-altitude satellite DEMETER, *J. Geophys. Res. Space Physics*, *119*, doi:10.1002/2013JA019557.

Received 19 OCT 2013
Accepted 27 FEB 2014
Accepted article online 4 MAR 2014

Analysis of fine ELF wave structures observed poleward from the ionospheric trough by the low-altitude satellite DEMETER

Michel Parrot[1], František Němec[2], and Ondřej Santolík[2,3]

[1]LPC2E/CNRS, Orléans, France, [2]Faculty of Mathematics and Physics, Charles University, Prague, Czech Republic, [3]Institute of Atmospheric Physics AS CR, Prague, Czech Republic

Abstract DEMETER was a three-axis stabilized Earth-pointing spacecraft launched on 29 June 2004 into a low-altitude (710 km) polar and circular orbit that was subsequently lowered to 650 km until the end of the mission in December 2010. DEMETER measured electromagnetic waves all around the Earth except at magnetic invariant latitudes >65°. The frequency range for the electric field was from DC up to 3.5 MHz and for the magnetic field from a few hertz up to 20 kHz. Electromagnetic ion cyclotron (EMIC) waves have been previously observed by DEMETER close to the ionospheric trough during high magnetic activity, and this paper describes another type of EMIC waves. These waves are also observed close to the trough, but they extend poleward, with the trough acting as a boundary. They are observed exclusively during the night and preferentially during geomagnetic substorms. The analysis of wave propagation shows that they propagate nearly along the ambient magnetic field and that they come from larger radial distances.

1. Introduction

This paper is related to the description of electromagnetic ELF emissions observed at low altitudes and at the highest geomagnetic latitudes covered by the spacecraft. It can be considered as a complement of the paper by *Parrot et al*. [2006b] because these two papers deal with waves registered close to the ionospheric trough by the same low-altitude microsatellite DEMETER. The emissions are detected in the ELF range (200 Hz to 3 kHz) in the upper ionosphere during geomagnetic substorms, and it is shown that they could be related to electromagnetic ion cyclotron (EMIC) waves.

EMIC waves have been studied with ground and satellite experiments, and references to these previous studies are given by *Parrot et al*. [2006b]. They have been observed in association with intense electron fluxes on auroral field lines by various satellites, and they have been also observed in the equatorial plane at various *L* values. In the equatorial region, EMIC waves are generated from the ion cyclotron instability driven by the anisotropic distribution of ring current energetic ions during magnetic storms. They are characterized by harmonic structures with electric and magnetic field power between the first multiples of ion cyclotron frequencies.

The aim of this paper is to use data from the low-altitude satellite DEMETER to study the ELF wave structures, which occur poleward of the ionospheric trough and to show the difference from the waves described by *Parrot et al*. [2006b]. The DEMETER payload is briefly described in section 2. In section 3, a few events are shown together with their common characteristics. A wave propagation analysis is presented in section 4 with discussions. Conclusions are provided in section 5.

2. The DEMETER Experiments

DEMETER was a low-altitude satellite launched in June 2004 onto a polar and circular orbit that measured electromagnetic waves and plasma parameters all around the globe except at magnetic invariant latitudes >65° [*Cussac et al*., 2006]. Its initial altitude of ~710 km was lowered to ~660 km at the end of 2005 until the end of the mission in December 2010. The orbit was nearly Sun synchronous with an ascending node at 22.30 LT in the night sector and a descending node at 10.30 LT during daytime.

There were two scientific modes: (i) a survey mode where spectra of one electric and one magnetic component are onboard computed up to 20 kHz with a frequency resolution of 19.53 Hz and a time

©2014. American Geophysical Union. All Rights Reserved.

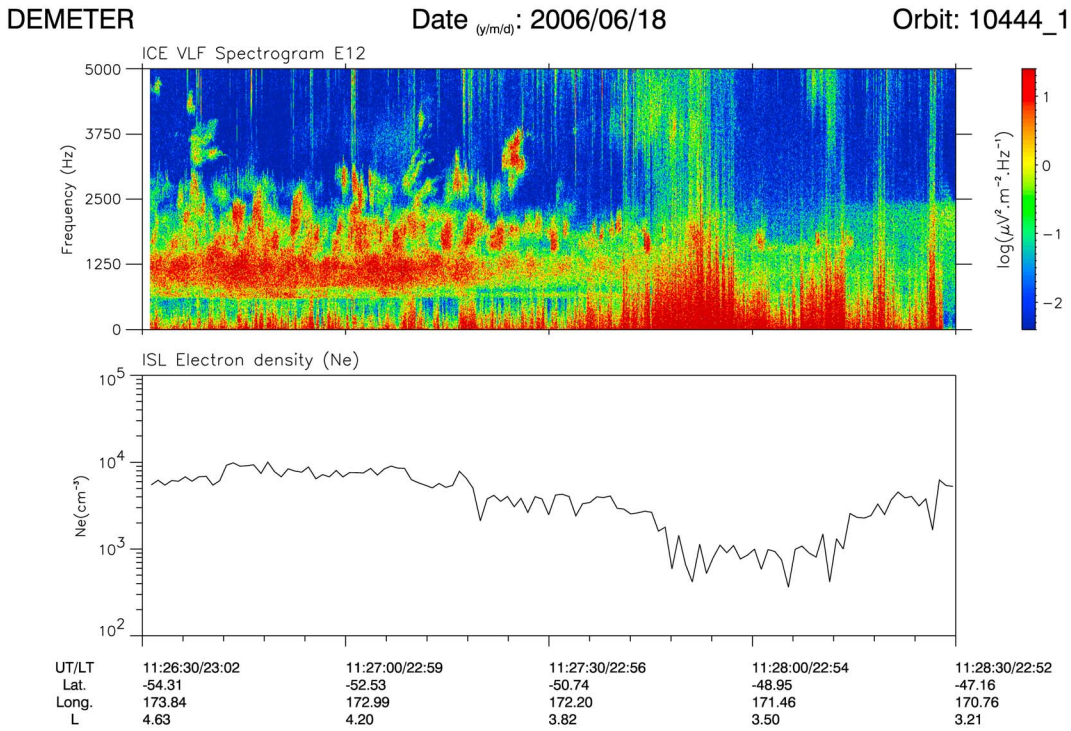


Figure 1. (top) Electric VLF spectrogram recorded on 18 June 2006 between 11:26:30 UT and 11:28:30 UT. The spectrogram is from 0 up to 5 kHz, and its intensity is color coded according to the scale on the right. (bottom) Electron density during the same time interval. The parameters displayed below are the time in UT, the local time (LT), the geographic latitude and longitude, and the McIlwain parameter *L*.

resolution of 2 s and (ii) a burst mode where waveforms of one electric and one magnetic component are recorded up to 20 kHz, and waveforms of the six electromagnetic field components are recorded up to 1.25 kHz. Details of the wave experiment can be found in *Berthelier et al*. [2006] and in *Parrot et al*. [2006a]. The burst mode, which is triggered above predetermined regions, allows us to perform a spectral analysis with a better frequency resolution. It is also possible to achieve wave propagation analysis with the six components of the wavefield. For this purpose, a relevant software named PRASSADCO previously used for past missions has been adapted to process the DEMETER data [*Santolík et al*., 2006].

The electron density data used in this paper were recorded by the ISL (Instrument Sonde de Langmuir) experiment onboard the satellite. The time resolution is 1 s. Details about ISL can be found in *Lebreton et al*. [2006].

The payload was nearly continuously operated at invariant latitudes below 65°, but dedicated operations were also programmed at higher latitudes when the satellite was flying over ground-based facilities such as European Incoherent Scatter (EISCAT) or High Frequency Active Auroral Research Program (HAARP) [see, for example, *Piddyachiy et al*., 2008].

3. The Events

The first event is shown in Figure 1. Figure 1 (top) represents the electric field spectrogram up to 5 kHz, whereas Figure 1 (bottom) is devoted to the electron density. A decrease of the electron density can be observed after 11:27:30 UT, corresponding to the occurrence of strong electrostatic turbulence in the electric field spectrogram. This indicates the position of the ionospheric trough known to be linked to the plasmapause at higher altitudes [*Yizengaw et al*., 2005; *Piddyachiy et al*., 2011]. On the left of this trough, i.e., in the direction toward higher latitudes, one can see wave structures and lines from 600 Hz up to 3 kHz. These are the fine ELF structures that are analyzed in this work. Figure 2 displays another example to indicate that these are electromagnetic waves (see also section 4). Figure 2 (top) shows the electric field spectrogram up to

©2014. American Geophysical Union. All Rights Reserved.

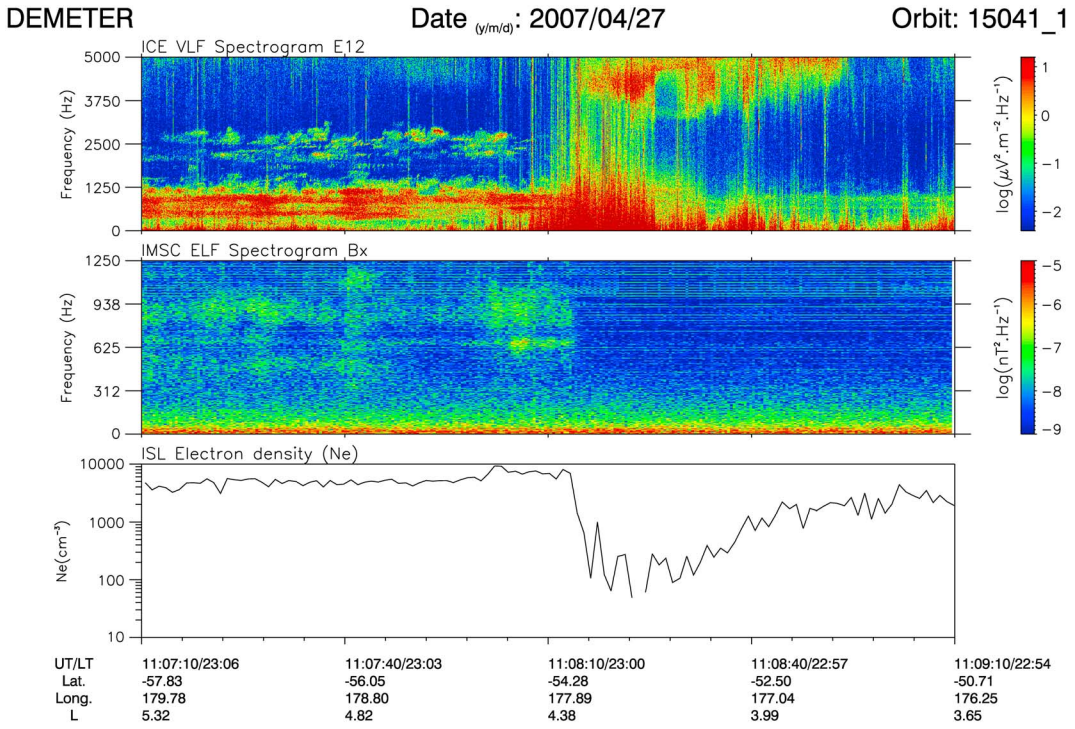


Figure 2. (top) Electric VLF spectrogram recorded on 27 April 2007 between 11:07:10 UT and 11:09:10 UT. The spectrogram is from 0 up to 5 kHz. (middle) Magnetic ELF spectrogram during the same time interval from 0 up to 1250 Hz. The intensities of the spectrograms are color coded according to the scales on the right. (bottom) Electron density during the same time interval. The parameters displayed below are the time in UT, the local time, the geographic latitude and longitude, and the McIlwain parameter *L*.

5 kHz, Figure 2 (middle) shows the magnetic field spectrogram up to 1.25 kHz (the data are polluted by interferences at higher frequencies), and Figure 2 (bottom) shows the electron density. The trough is again well defined just after 11:08:10 UT, and constant frequency wave structures can be observed on the left-hand side (poleward) of it at frequencies up to 3.0 kHz. Two last examples are given in Figure 3 which displays electric field spectrograms with the full VLF range, i.e., up to 20 kHz. In the two panels, the position of the trough corresponds to the occurrence of electrostatic turbulence (around 10:55:45 UT in Figure 3 (top) and 11:14:37 UT in Figure 3 (bottom)). At low frequencies, these wave structures with lines are observed on the left-hand side (poleward) of the trough (in the frequency range from 300 Hz to 2.6 kHz in Figure 3 (top) and from 300 Hz to 3.3 kHz in Figure 3 (bottom)), whereas on the equatorward side of it, a broadband noise, which covers the same frequency band, can be seen. This broadband noise corresponds to plasmaspheric hiss, which is also bounded by the trough but at lower latitudes inside the plasmasphere. In Figure 3 (bottom), the poleward wave structures are much more complicated as they can be observed at frequencies larger than 5 kHz. In the upper part of the two spectrograms, one can observe spectral lines corresponding to ground-based VLF transmitters.

Figure 4 displays the locations of 92 events, which have been observed during the DEMETER lifetime. The number of identified events is far from being representative of the real number of events, which can be expected with a polar orbiting satellite. This is due to the fact that DEMETER did not properly cover the high latitudes and that only the data recorded during burst mode operation have been visually checked (the burst mode coverage is color coded in Figure 4). The frequency resolution of the survey mode is generally insufficient for a proper identification of this type of waves. Nevertheless, Figure 4 shows that there is no clear longitudinal dependence and that these events can be equally observed at high latitudes in the north and in the south. Many of the events were observed when the DEMETER burst mode was extended for experiments with HAARP, HAARP conjugate, and EISCAT [see, for example, *Piddyachiy*, 2012]. Several of these observations occurred when DEMETER is beyond its normal invariant latitude of 65°. It is

©2014. American Geophysical Union. All Rights Reserved.

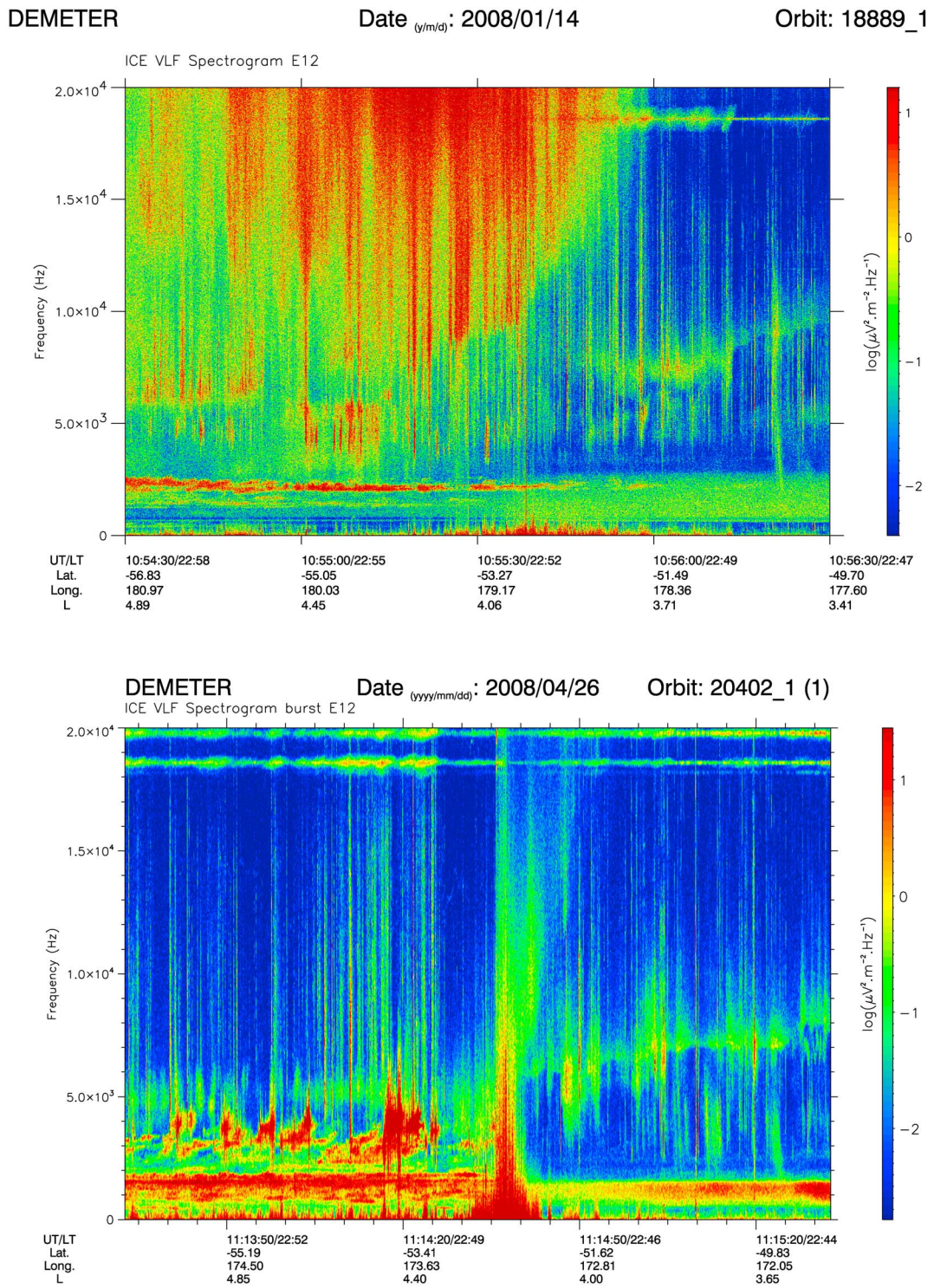


Figure 3. (top) Electric VLF spectrogram recorded on 14 January 2008 between 10:54:30 UT and 10:56:30 UT. (bottom) Electric VLF spectrogram recorded on 26 April 2008 between 11:13:35 UT and 11:15:35 UT. The spectrograms are from 0 up to 20 kHz, and their intensities are color coded according to the scales on the right. The parameters displayed below are the time in UT, the local time, the geographic latitude and longitude, and the McIlwain parameter *L*.

©2014. American Geophysical Union. All Rights Reserved.

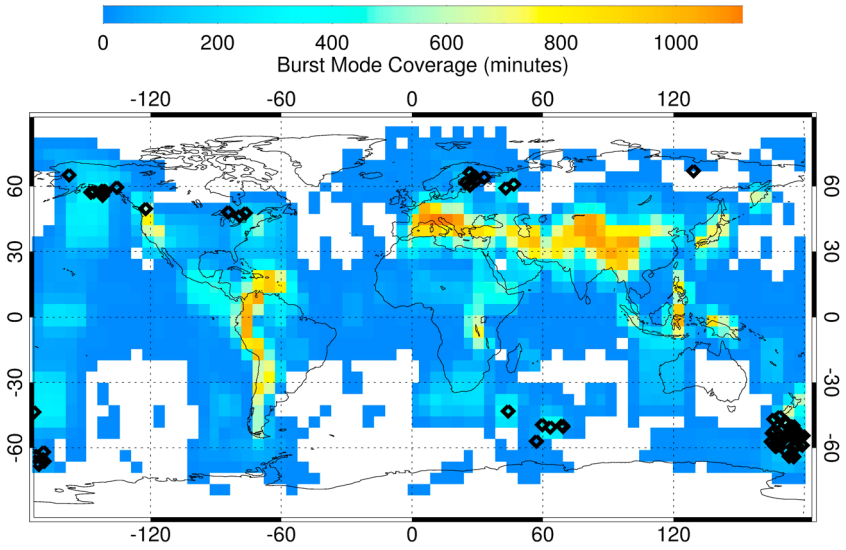


Figure 4. Geographical occurrence of the 92 events observed during the lifetime of the mission (black diamonds). The map also shows the burst mode coverage according to the color scale at the top.

likely that if burst modes were implemented in other high-latitude regions, then such events would also be observed at other longitudes.

It is of a great importance to investigate whether the geomagnetic conditions during the occurrence of the events differ from the normal ones or not. We have therefore used a superposed epoch analysis to determine the correlation between the timing of these events and the value of the *AE* index. The time resolution used for the analysis was set to 1 h. The results are shown in Figure 5. The thick line represents the dependence obtained for the mean value of the *AE* index, while the standard deviation of this mean value is marked by thin lines. It can be seen that there is a statistically significant increase of the *AE* index at the time of the events, on average by about 300 nT as compared to normal values. This means that the events are observed predominantly during geomagnetic substorms.

Observations therefore indicate that these fine ELF wave structures are a common phenomena during sustained auroral activity. One must also notice that all the 92 events have been recorded during nighttime, while HAARP and HAARP conjugate extensions were done approximately equivalently for daytime and nighttime (a set of statistics is shown in Figure 5.1 of *Piddyachiy* [2012]).

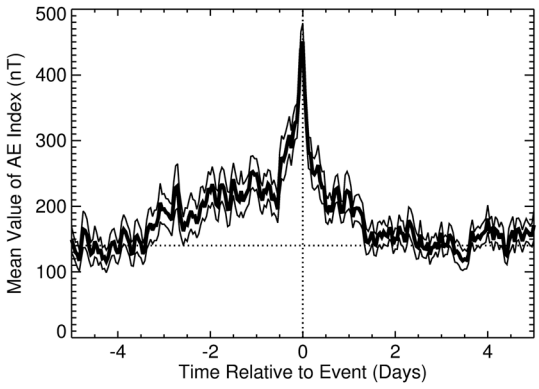


Figure 5. Results of the superposed epoch analysis of the *AE* index. Its mean value (bold) as a function of the time relative to the occurrence of the 92 events and standard deviation of the mean value (thin). The vertical dotted line shows zero time difference, and the horizontal dotted line shows the usual average *AE* value in absence of the events.

4. Wave Analysis and Discussions

These ELF waves are electromagnetic because both electric and magnetic intensities of the emissions are high. Consequently, it is possible to determine the propagation characteristics of waves observed at frequencies lower than 1.25 kHz from burst mode data, when the six components of the electromagnetic field are available (see section 2). Figures 6 and 7 show the wave propagation analysis of the two burst mode events from Figures 1 and 2, respectively. The individual panels are the same from first panel to sixth panel for the two figures. Frequency-time spectrograms of the magnetic and electric field fluctuations are shown in the

©2014. American Geophysical Union. All Rights Reserved.

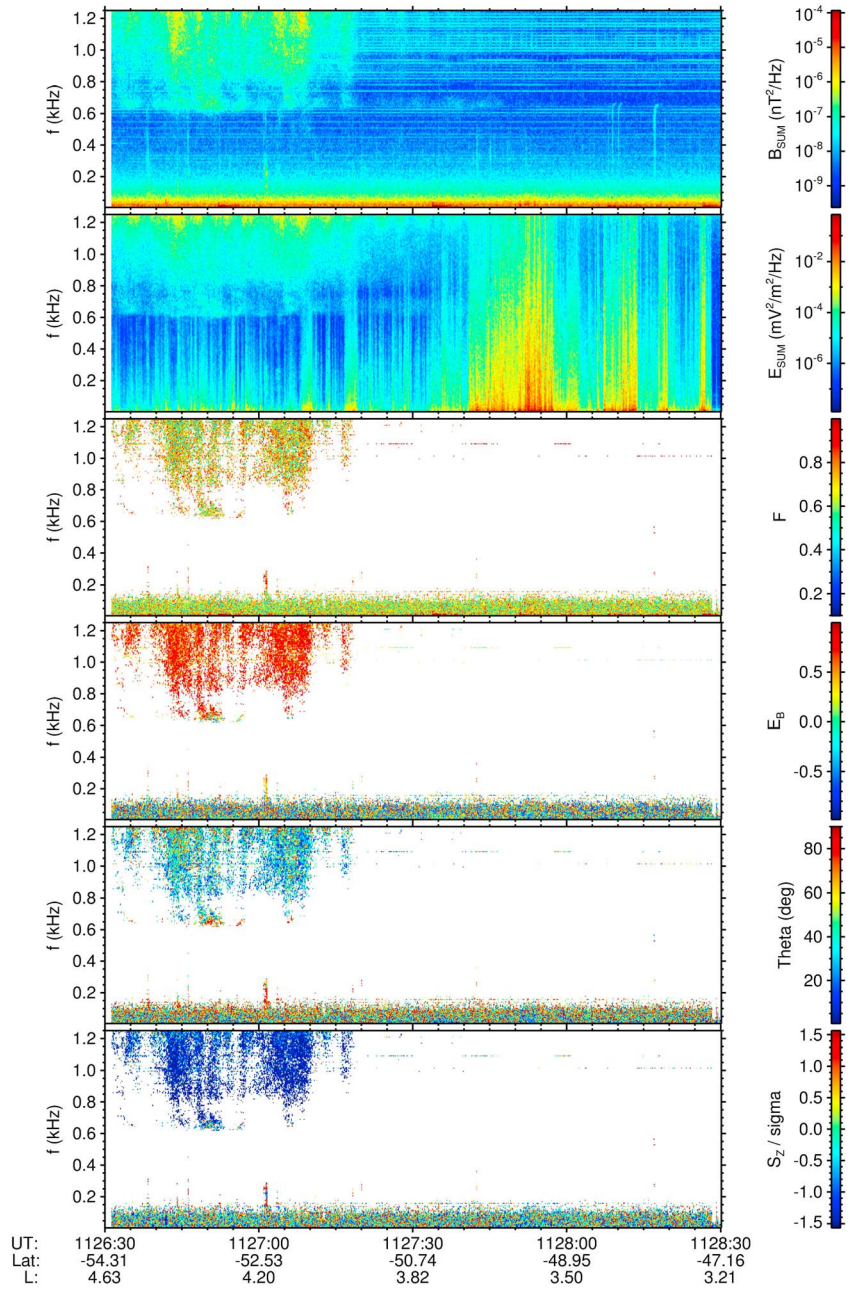


Figure 6. Wave propagation analysis of the event shown in Figure 1. (top to bottom) The magnetic field spectrogram, the electric field spectrogram, the planarity of polarization of the wave magnetic field, the ellipticity, the polar angle θ, and the Poynting vector component along the terrestrial magnetic field normalized by the standard deviation (see text for explanation). All parameters are color coded according to the scales on the right. The frequency range is up to 1250 Hz. The parameters displayed on the abscissa are the time in UT, the geomagnetic latitude, and the McIlwain parameter *L*.

first two panels. The third panel displays the parameter *F* which is the planarity of polarization of the wave magnetic field (this parameter characterizes the degree of similarity of the wave polarization with the ideal polarization of a single plane wave). The fourth panel represents E_B, the ellipticity (ratio of the axes of the polarization ellipse) calculated from the magnetic field polarization data using the singular value decomposition (SVD) method [*Santolík et al.*, 2003]. The sign of E_B represents the information about the sense of polarization with respect to the stationary magnetic field. Negative values are used for left-handed polarization sense and positive values for the right-handed polarization sense. The same SVD method is also used to calculate the direction of the wave vector. The fifth panel shows the wave normal

©2014. American Geophysical Union. All Rights Reserved.

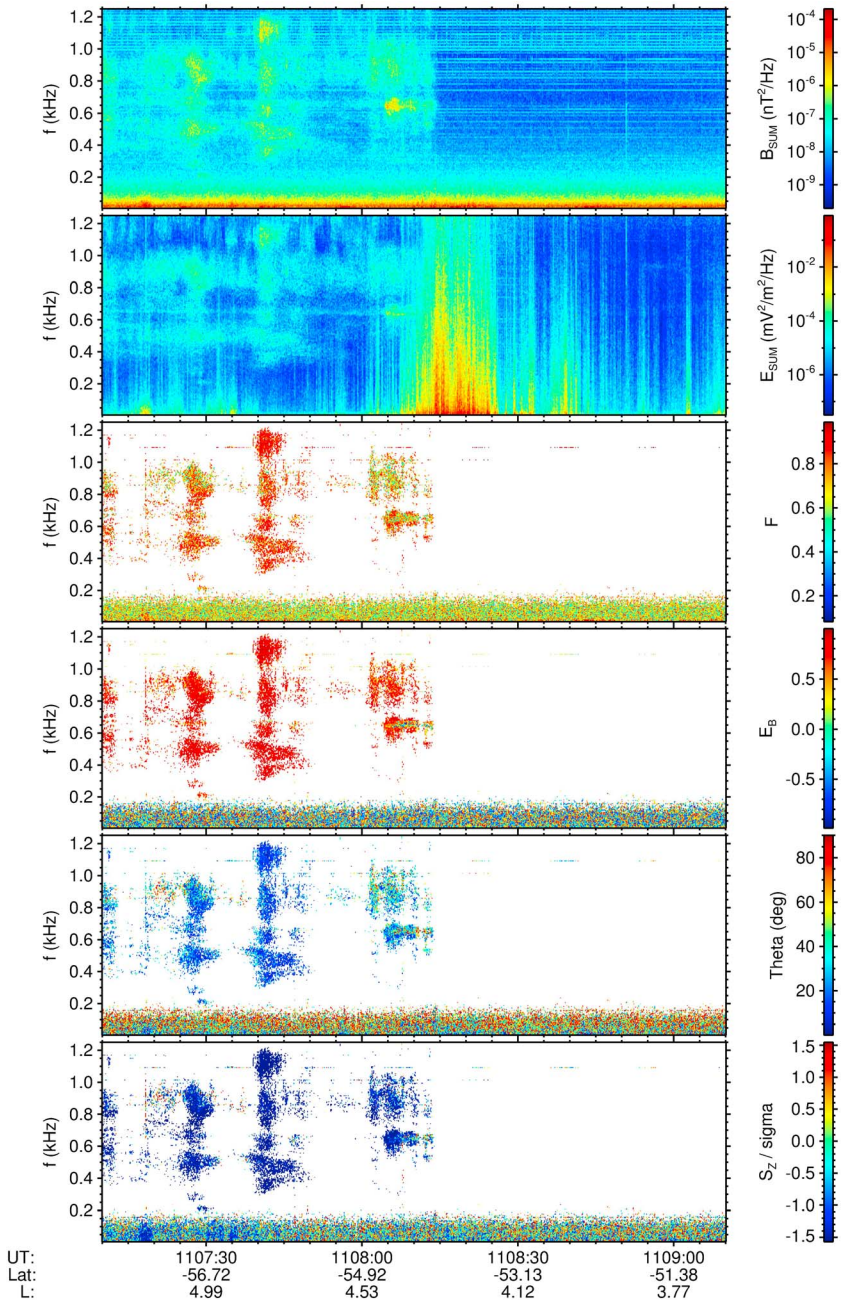


Figure 7. Same parameters as in Figure 6 but for the event from Figure 2.

angle θ defined as the angle between the Earth's magnetic field and the wave vector. The sixth panel gives the Poynting vector component along the terrestrial magnetic field normalized by its standard deviation resulting from the statistical errors of the spectral analysis. The empty areas in the panels correspond to frequency-time intervals with magnetic power spectral densities below $10^{-7}\,\mathrm{nT^2\,Hz^{-1}}$ or electric power spectral densities below $10^{-6}\,\mathrm{mV^2\,m^{-2}\,Hz^{-1}}$. These areas are empty because the analysis is not meaningful for low-power waves.

The results of this multidimensional analysis of plasma wave measurements as a function of the universal time (UT) and frequency indicate for the two events that the waves are quasi field-aligned (low θ values), right-handed circularly polarized (E_B is close to +1), and propagating in the opposite direction of the Earth's magnetic field. As both events take place in the Southern Hemisphere, it means that the waves are

©2014. American Geophysical Union. All Rights Reserved.

propagating away from the geomagnetic equator. Qualitatively, similar results were obtained for all remaining events for which a detailed wave analysis was possible.

In Figure 6, the magnetic power spectral density is on the order of $2. \times 10^{-6}\,nT^2\,Hz^{-1}$, and the electric power spectral densities on the order of $10^{-3}\,mV^2\,m^{-2}\,Hz^{-1}$ at 1.2 kHz. A rough estimation of the *E/B* ratio gives $2. \times 10^7\,m\,s^{-1}$, and therefore, it confirms that these emissions are electromagnetic waves.

The detailed spectral analysis indicates that the events are sometimes composed of several spectral lines. Past observations have shown that such structures in the auroral region or in the equatorial region could be related to EMIC waves. It is known on one hand, that these waves are guided by steep density gradients near the plasmapause [*Kasahara et al*., 1994; *Thorne and Horne*, 1997; *Fraser and Nguyen*, 2001] and on the other hand, that the ionospheric trough is linked to the plasmapause at higher altitudes [*Yizengaw et al*., 2005].

The waves appear on the poleward border of these regions, and therefore, it is expected that the events observed in the ionosphere by DEMETER are linked to EMIC waves at ion cyclotron harmonics similar to the waves observed in a different auroral zone by *Chaston et al*. [2002] or *Santolík et al*. [2002b]. However, in the DEMETER events, the propagation analysis does not exclude the possibility that the waves originate from the equatorial region (see the ray-tracing analysis in Appendix A). They could be related to the emissions observed in the equatorial region at much larger *L* values by *Santolík et al*. [2002a], who observed with CLUSTER harmonic lines at frequencies higher than 9 times the proton gyrofrequency. The emissions observed by *Santolík et al*. [2002b] were near the local proton gyrofrequency and its lowest harmonics and therefore in a different frequency range (<200 Hz) than those reported here. Moreover, our events do not have a link with the local proton gyrofrequency, which is on the order of 680 Hz both in Figure 1 (at 11:27:00 UT) and Figure 2 (at 11:07:30 UT). The emissions presented here are also not so regular as the electromagnetic ion cyclotron waves observed up to 1 kHz by *Chaston et al*. [2002]. They are different from the frequency-banded electromagnetic VLF waves up to 2 kHz observed by *Colpitts et al*. [2012] during large magnetic storms (not the same structure, not the same location, and not the same magnetic activity), although these VLF waves are also attributed to ions.

As shown in *Parrot et al*. [2006b], it is assumed that waves with frequencies equal to multiples of the ion gyrofrequencies are emitted in the equatorial plane at lower *L* values. They bounce from one hemisphere to another, and when they find a density gradient, which corresponds to the plasmapause location, they propagate down to the ionosphere, where they are observed by DEMETER in both hemispheres. The numerous spectral lines which are observed and their broadening may be due to scattering from ionospheric irregularities (enhanced by the magnetic activity) during the wave propagation [see, for example, *Bell et al*., 2008].

The two events shown in Figure 3 also indicate that the trough is a clear boundary for the plasmaspheric hiss (see the review by *Hayakawa and Sazhin* [1992]) in the ionosphere at low altitudes.

5. Conclusions

New observation of ELF waves with line structures has been performed by the low-altitude DEMETER microsatellite in the high-latitude ionosphere. The main differences from the previous observations by *Parrot et al*. [2006b] are as follows:

1. These intense EM waves are observed during moderate magnetic storms at frequencies between 500 Hz and 2.5 kHz.
2. They are only observed during nighttime.
3. They are not limited to regions close to the trough as they extend poleward.
4. In their occurrence zones, they appear to propagate with a direction aligned with the magnetic field. They have line structures but without clear harmonics.
5. They can be linked to EMIC waves at ion cyclotron harmonics emitted from the auroral zone or from the equatorial region, bouncing in the magnetosphere and propagating down to the ionosphere, because they follow density gradients (plasmapause).

Appendix A: Ray-Tracing Analysis

To check the possibility that these waves have their origin in the equatorial region, results from Figure 6 have been used as inputs of a ray-tracing program used to trace back the ray to the source. We use the

©2014. American Geophysical Union. All Rights Reserved.

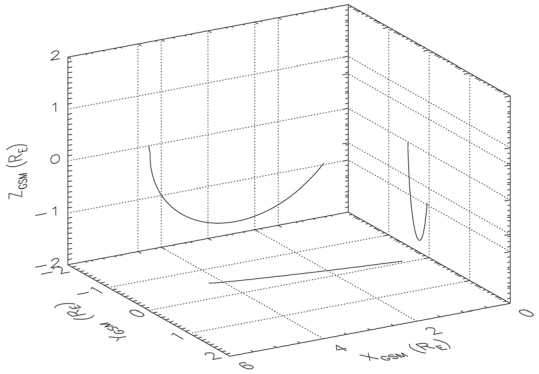


Figure A1. Results of a ray-tracing analysis using the conditions of Figures 1 and 6 and represented in a GSM system. In order to have a better display of the ray trajectory, the 3-D plot is projected on the three planes: *XY*, *XZ*, and *YZ*.

three-dimensional procedure of *Cerisier* [1970], which was also utilized by *Cairo and Lefeuvre* [1986], *Muto and Hayakawa* [1987], and *Parrot et al*. [2003]. The ray-tracing software uses a dipolar approximation of the magnetic field and a diffusive equilibrium model for ion and electron densities including a plasmapause *L*-central position at 4.2 and a plasmapause *L*-half width equal to 0.4. The satellite is located in the South Hemisphere (latitude = −50°, longitude = 173°), and the initial conditions at its altitude (660 km) are $f = 1.5$ kHz and $\theta = 10°$. Figure A1 represents the three-plane projections of the ray plot in 3-D using a GSM (geocentric solar magnetospheric) system. It can be seen that the ray is able to reach the equator ($Z_{GSM} = 0$). This is possible because a plasmapause model was included in the software (at the equator, it is observed that the *L* value is close to 4.3).

Acknowledgments

This work was supported by the Centre National d'Etudes Spatiales. It is based on observations with the electric field instrument ICE, the magnetic field instrument IMSC, and the Langmuir probe ISL aboard DEMETER. The authors thank J.J. Berthelier and J.P. Lebreton, the PIs of ICE and ISL, for the use of the data. The work of F.N. was supported by GACR grant P209/12/P658. O.S. was supported by GACR grant 205/10/2279 and MSMT grant LH12231.

Robert Lysak thanks Denys Piddyachiy and another reviewer for their assistance in evaluating this paper.

References

Bell, T. F., U. S. Inan, D. Piddyachiy, P. Kulkarni, and M. Parrot (2008), Effects of plasma density irregularities on the pitch angle scattering of radiation belt electrons by signals from ground based VLF transmitters, *Geophys. Res. Lett.*, *35*, L19103, doi:10.1029/2008GL034834.

Berthelier, J. J., et al. (2006), ICE, the electric field experiment on DEMETER, *Planet. Space Sci.*, *54*, 456–471, doi:10.1016/j.pss.2005.10.016.

Cairo, L., and F. Lefeuvre (1986), Localization of sources of ELF/VLF hiss observed in the magnetosphere: Three-dimensional ray tracing, *J. Geophys. Res.*, *91*, 4352–4364.

Cerisier, J. C. (1970), Propagation perpendiculaire au voisinage de la fréquence de la résonance hybride basse, in *Plasma Waves in Space and in the Laboratory*, vol. 2, pp. 487–521, Edinburgh Univ. Press, Edinburgh, Scotland.

Chaston, C. C., J. W. Bonnell, J. P. McFadden, R. E. Ergun, and C. W. Carlson (2002), Electromagnetic ion cyclotron waves at proton cyclotron harmonics, *J. Geophys. Res.*, *107*(A11), 1351, doi:10.1029/2001JA900141.

Colpitts, C. A., C. A. Cattell, J. U. Kozyra, and M. Parrot (2012), Satellite observations of banded VLF emissions in conjunction with energy-banded ions during very large geomagnetic storms, *J. Geophys. Res.*, *117*, A10211, doi:10.1029/2011JA017329.

Cussac, T., M. A. Clair, P. Ultré-Guerard, F. Buisson, G. Lassalle-Balier, M. Ledu, C. Elisabelar, X. Passot, and N. Rey (2006), The DEMETER microsatellite and ground segment, *Planet. Space Sci.*, *54*(5), 413–427.

Fraser, B. J., and T. S. Nguyen (2001), Is the plasmapause a preferred source region of electromagnetic ion cyclotron waves in the magnetosphere?, *J. Atmos. Sol. Terr. Phys.*, *63*, 1225–1247.

Hayakawa, M., and S. S. Sazhin (1992), Mid-latitude and plasmaspheric hiss: A review, *Planet. Space Sci.*, *40*, 1325.

Kasahara, Y., H. Kenmochi, and I. Kimura (1994), Propagation characteristics of the ELF emissions observed by the satellite Akebono in the magnetic equatorial region, *Radio Sci.*, *29*, 751–767.

Lebreton, J. P., et al. (2006), The ISL Langmuir probe experiment processing onboard DEMETER: Scientific objectives, description and first results, *Planet. Space Sci.*, *54*, 472–486.

Muto, H., and M. Hayakawa (1987), Ray-tracing study of the propagation in the magnetosphere of whistler-mode VLF emissions with frequency above one half the gyrofrequency, *Planet. Space Sci.*, *35*, 1397–1404.

Parrot, M., O. Santolík, N. Cornilleau-Wehrlin, M. Maksimovic, and C. Harvey (2003), Magnetospherically reflected chorus emissions revealed by ray tracing with CLUSTER data, *Ann. Geophys.*, *21*(5), 1111–1120.

Parrot, M., et al. (2006a), The magnetic field experiment IMSC and its data processing onboard DEMETER: Scientific objectives, description and first results, *Planet. Space Sci.*, *54*, 441–455, doi:10.1016/j.pss.2005.10.015.

Parrot, M., A. Buzzi, O. Santolík, J. J. Berthelier, J. A. Sauvaud, and J. P. Lebreton (2006b), New observations of electromagnetic harmonic ELF emissions in the ionosphere by the DEMETER satellite during large magnetic storms, *J. Geophys. Res.*, *111*, A08301, doi:10.1029/2005JA011583.

Piddyachiy, D. (2012), Propagation of ELF Waves Generated by an HF Ionospheric Heater in the Earth's Plasma Environment, Stanford Univ., PhD thesis.

Piddyachiy, D., U. S. Inan, T. F. Bell, N. G. Lehtinen, and M. Parrot (2008), DEMETER observations of an intense upgoing column of ELF/VLF radiation excited by the HAARP HF heater, *J. Geophys. Res.*, *113*, A10308, doi:10.1029/2008JA013208.

Piddyachiy, D., T. F. Bell, J. J. Berthelier, U. S. Inan, and M. Parrot (2011), DEMETER observations of the ionospheric trough over HAARP in relation to HF heating experiments, *J. Geophys. Res.*, *116*, A06304, doi:10.1029/2010JA016128.

Santolík, O., J. S. Pickett, D. A. Gurnett, M. Maksimovic, and N. Cornilleau-Wehrlin (2002a), Spatiotemporal variability and propagation of equatorial noise observed by Cluster, *J. Geophys. Res.*, *107*(A12), 1495, doi:10.1029/2001JA009159.

Santolík, O., J. S. Pickett, D. A. Gurnett, and L. R. O. Storey (2002b), Magnetic component of narrow-band ion cyclotron waves in the auroral zone, *J. Geophys. Res.*, *107*(A12), 1444, doi:10.1029/2001JA000146.

Santolík, O., M. Parrot, and F. Lefeuvre (2003), Singular value decomposition methods for wave propagation analysis, *Radio Sci.*, *38*(1), 1010, doi:10.1029/2000RS002523.

Santolík, O., F. Němec, M. Parrot, D. Lagoutte, and L. Madrias (2006), Analysis methods for multi-component wave measurements on board the DEMETER spacecraft, *Planet. Space Sci.*, *54*, 512–527, doi:10.1016/j.pss.2005.10.020.

Thorne, R. M., and R. B. Horne (1997), Modulation of electromagnetic ion cyclotron instability due to the interaction with ring current O+ during magnetic storms, *J. Geophys. Res.*, *102*, 14,155–14,164.

Yizengaw, E., H. Wei, M. B. Moldwin, D. Galvan, L. Mandrake, A. Mannucci, and X. Pi (2005), The correlation between midlatitude trough and the plasmapause, *Geophys. Res. Lett.*, *32*, L10102, doi:10.1029/2005GL022954.

©2014. American Geophysical Union. All Rights Reserved.